PHYSICS

Emergent stereoselective interactions and self-recognition in polar chiral active ellipsoids

Pragya Arora[1]*, A. K. Sood[2,3], Rajesh Ganapathy[3,4]*

In many active matter systems, particle trajectories have a well-defined handedness or chirality. Whether such chiral activity can introduce stereoselective interactions between particles is not known. Here, we developed a strategy to tune the nature of chiral activity of three-dimensionally printed granular ellipsoids without altering their shape or size. In vertically agitated monolayers of these particles, we observed two types of dimers form depending on the chirality of the pairing monomers. Heterochiral dimers moved collectively as a single achiral active unit, while homochiral ones formed a translationally immobile spinner. In active racemic mixtures, the former was more abundant than the latter, indicating that interactions were stereoselective. Through dimer lifetime measurements, we further provide evidence for chiral self-recognition in mixtures of particles with different chiral activities. We lastly show that, at fixed particle number density, changing the net chirality of a dense active liquid fundamentally alters the nature of collective relaxation.

INTRODUCTION

When chirality is present as a static feature of building blocks, interactions between and reactions involving them are often stereoselective (*1*). For molecular building blocks, chirality also leads to higher-order effects such as self-recognition, sorting, and discrimination (*2*). There are, however, many instances where chirality is also manifest in the dynamics. Examples in the realm of classical physics where particle trajectories have a chirality/handedness associated with them include assemblies of spinning colloidal magnets (*3*, *4*) and granules (*5*), spinning (*6*) and circularly swimming bacteria (*7*) in the vicinity of walls, spiral (*8*) and helical swimmers (*9*), and synthetic chiral active particles (*10*–*13*). In one of these systems—magnetic disks set spinning by a rotating external field—where chirality was present in both the particle shape and dynamics, emergent stereoselective interactions between particles was observed to aid in their dynamic self-assembly (*5*). A rather fundamental question then is whether such interactions, and maybe even self-recognition, can emerge in a system where chirality is only a feature of the dynamics. Systems like the one studied in (*5*) are immediately ruled out, since all particles have the same handedness in their dynamics, which is set by the external rotating field, and when the particle shape is now made achiral, stereoselective interactions cannot even arise. These limitations, however, do not apply to active matter systems (*14*), since, here, the direction of motion, and also the handedness if activity is chiral (*15*), is set by the particle. In active matter ensembles sans attractive interparticle interactions, even achiral activity can result in notable collective behavior (*14*) and also lead to condensed phases (*16*, *17*). Even while chiral activity brings further richness to the dynamics (*13*, *18*, *19*), with numerical studies also anticipating chiral sorting (*20*), whether such an activity can mediate selectivity and recognition in these systems remains unanswered.

Addressing this question in experiments, even in two dimensions (2D), requires a system that provides some degree of control over chiral activity, and realizing this is not without its challenges. In 2D, the relevant parameters are the radius of the circular trajectory, R, and the angular velocity, ω, of the particle (*15*). Tuning either or both is difficult in living chiral active matter. While synthetic active spinners are easy to fabricate (*10*, *12*, *13*), being subject to only an active torque, $R = 0$, this constrains the parameter space of chiral activity. To realize the more generic circular trajectories, where both active torques and forces act, existing strategies for both wet and dry active matter rely on particle shapes that are chiral (*10*, *11*). Thus, within these approaches, disentangling emergent effects associated with chiral activity from those arising due to the chiral particle shape is virtually impossible.

RESULTS

Realizing tunable chiral active motion

Here, we achieved tunable chiral active motion while keeping the particle shape and size fixed and achiral by capitalizing on a hitherto unexploited feature of a canonical 2D active matter system—assemblies of millimeter-sized grains rendered active through vertical agitation. Previous experiments found that vibrated granules of simple shapes, like disks or rods, but with an asymmetry in mass, m, and/or friction coefficient, μ, were polar active along the direction set by the asymmetry (*21*–*23*). While, in these studies, when the asymmetry in both were present they were coincident, in our granules—3D-printed plastic ellipsoids—over and above an asymmetry in μ and m along the major axis, we also had an asymmetry in m along the minor axis. We anticipated vertical agitation to generate both an active force and torque on these particles and converged on this specific design after systematically excluding out other designs based on the nature of active dynamics observed (see fig. S4).

Our Janus ellipsoids had a major axis, $\alpha = 6$ mm, and minor axes, $\beta = 3$ mm and $\gamma = 2.1$ mm. We exploited a feature unique to the 3D print process to introduce a fore-aft asymmetry in μ, and this can be seen as a difference in the surface finish between the lower and upper half of the ellipsoid in Fig. 1 (A to F). A left-right asymmetry in m, with respect to the particle major axis, was achieved by making

[1]Chemistry and Physics of Materials Unit, Jawaharlal Nehru Centre for Advanced Scientific Research, Jakkur, Bangalore 560064, India. [2]Department of Physics, Indian Institute of Science, Bangalore 560012, India. [3]International Centre for Materials Science, Jawaharlal Nehru Centre for Advanced Scientific Research, Jakkur, Bangalore 560064, India. [4]School of Advanced Materials (SAMat), Jawaharlal Nehru Centre for Advanced Scientific Research, Jakkur, Bangalore 560064, India.
*Corresponding author. Email: pragyaarora26@gmail.com (P.A.); rajesh.ganapathy@gmail.com (R.G.)

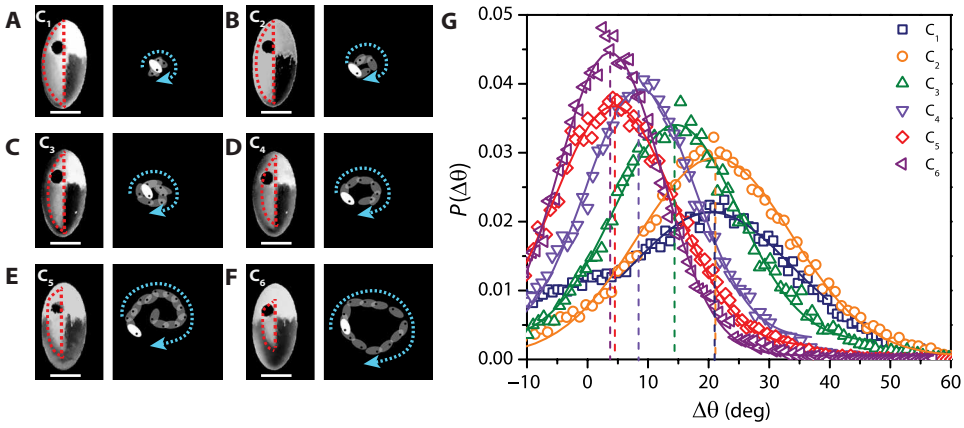

Fig. 1. Realizing tunable chiral active motion. (**A** to **F**) Left: Snapshots of 3D-printed chiral active ellipsoids for three different left-right mass asymmetries Δm_{LR}. The red dashed lines show the hollowed-out portion of the particle. Right: Superimposed snapshots showing a nearly circular path traced by the ellipsoids under vertical agitation. The snapshot of the ellipsoid at $t = 0$ s is shown in white. The blue arrows indicate the handedness of the orbit. Scale bars, 3 mm. (**G**) Probability distribution of angular displacements. Graph showing probability distribution of angular displacements $\Delta\theta$ between successive time instances ($\Delta t = 0.03$ s) of C_1 (blue □), C_2 (orange ○), C_3 (green △), C_4 (violet ▽), C_5 (red ◊), and C_6 (purple ◁). Photo credit: [(A) to (F), left panels] Pragya Arora, JNCASR.

one portion of the ellipsoid hollow during print (shown by dashed red lines in Fig. 1, A to F). The printed particles were placed on a horizontally mounted flower-shaped arena and confined from above with a transparent glass plate, which also enabled imaging of dynamics. The entire assembly was coupled to a permanent magnet shaker through a stiff air bearing, which ensured that the imposed sinusoidal driving from the shaker is channeled only into vertical oscillations of the plate (see Materials and Methods) (*24*). The drive frequency $f = 37$ Hz and amplitude $a = 1$ mm were kept constant in all experiments, unless specified, and the nondimensional acceleration $\Gamma = \frac{4\pi^2 f^2 a}{g} = 5.5$, where g is the acceleration due to gravity. We quantified the dynamics of individual ellipsoids by working at a very low area fraction $\phi \approx 0.1\%$ ($N \approx 8$ to 10 particles on the plate), where ϕ is the total projected area of all particles on the plate divided by the surface area of the plate. The energy gained by the particles through frequent collisions with the vibrating plate resulted in polar chiral active motion—noisy circular trajectories with a more or less well-defined R and ω (Fig. 1A, right, and movie S1). Since no special care was taken while placing particles on the plate, the granular assemblies were racemic mixtures and had nearly equal numbers of particles with dextrogyre [(+)] and levogyre [(−)] trajectories. Furthermore, as the gap between plates $\Delta = 2.4$ mm is such that $\gamma < \Delta < \beta$, particles cannot flip once they are confined, and the handedness of the orbits remained unchanged.

Now, by changing only the volume of the hollowed-out portion of the ellipsoid during 3D printing (red dashed lines in Fig. 1, A to F), we tuned the extent of left-right mass asymmetry, Δm_{LR}, and hence the active torque (see fig. S5). We tracked the dynamics of many individual ellipsoids for a given Δm_{LR} and determined the probability distribution of angular displacements $P(\Delta\theta)$ between successive time instances ($\Delta t = 0.03$ s). $P(\Delta\theta)$ was Gaussian for all the mass asymmetries studied, and its peak shifted to smaller $\Delta\theta$ with Δm_{LR} (Fig. 1G). As anticipated, decreasing Δm_{LR} resulted in a smaller active torque and thus a decrease in ω and an increase in R (right panels in Fig. 1, A to F). Ellipsoids with different Δm_{LR} values are labeled C_1 to C_6, where a larger subscript indicates a larger R (see Table 1).

Emergent stereoselective interactions in polar chiral active ellipsoids

Having gained the ability to tune chiral activity, we investigated dynamics of the granular assemblies at higher ϕ. Even at a ϕ as low as 1%, we observed dimer formation solely due to chiral activity. We observed qualitatively similar dynamics for C_1 and C_2 ellipsoids. In racemic mixtures of these particles, we observed two distinct types of active dimers, which we classified as "movers" and "spinners" based on their dynamics. This difference in behavior was entirely a consequence of their composition. The mover was made of a (+) and a (−) monomer with their polar axis pointing in nearly the same direction, and the adduct largely behaved like an achiral polar active particle (movie S2). Figure 2A shows the representative experimental trajectory of a mover made of C_2 monomers. The translational mean squared displacement (MSD) of the center of mass (COM) of the adduct was superdiffusive at small lag times t and then crossed over to diffusive dynamics at larger t (solid black symbols in Fig. 2C) (*25*). However, the orientational MSD of movers was superdiffusive at longer times, indicating that the movers experienced some residual torque (fig. S6). In contrast, a spinner was made of monomers that were both (+) or both (−) but whose polar axis pointed in opposite directions (see Fig. 2B and movie S3 for a spinner made of C_2 monomers). The orientational MSD of the spinners showed a crossover from superdiffusive to ballistic behavior with t (red circles in Fig. 2C). Because of the almost complete cancellation of the active forces, the translational dynamics of the spinner was purely diffusive with a diffusion constant that was nearly two orders of magnitude smaller than that of the movers (fig. S7).

Such mover and spinner states are theoretically predicted for two hydrodynamically interacting active rotors (*26*). However, it is not known whether, in a racemic mixture of these rotors, one of these bound states is more abundant, which would then indicate active stereoselectivity (*2*). Hydrodynamic interactions, nevertheless, are not relevant for dry active matter. To determine whether, in our system, interactions were stereoselective, we calculated the fraction of dimers that existed as movers and spinners. In racemic

Table 1. Details of various 3D-printed polar chiral active ellipsoids.

Label	α (mm)	β (mm)	γ (mm)	Δm_{LR} (g)	ω (rad/s)	R (mm)	Dimer state observed
C_1	6	3	2.1	6.91×10^{-3}	12.2	1.3	Spinners, movers
C_2	6	3	2.1	5.85×10^{-3}	11.9	1.4	Spinners, movers
C_3	6	3	2.1	4.78×10^{-3}	8.5	2.2	Movers
C_4	6	3	2.1	3.13×10^{-3}	5.1	4.1	Movers
C_5	6	3	2.1	1.97×10^{-3}	2.5	6.1	Movers
C_6	6	3	2.1	1.04×10^{-3}	2.1	10	Movers

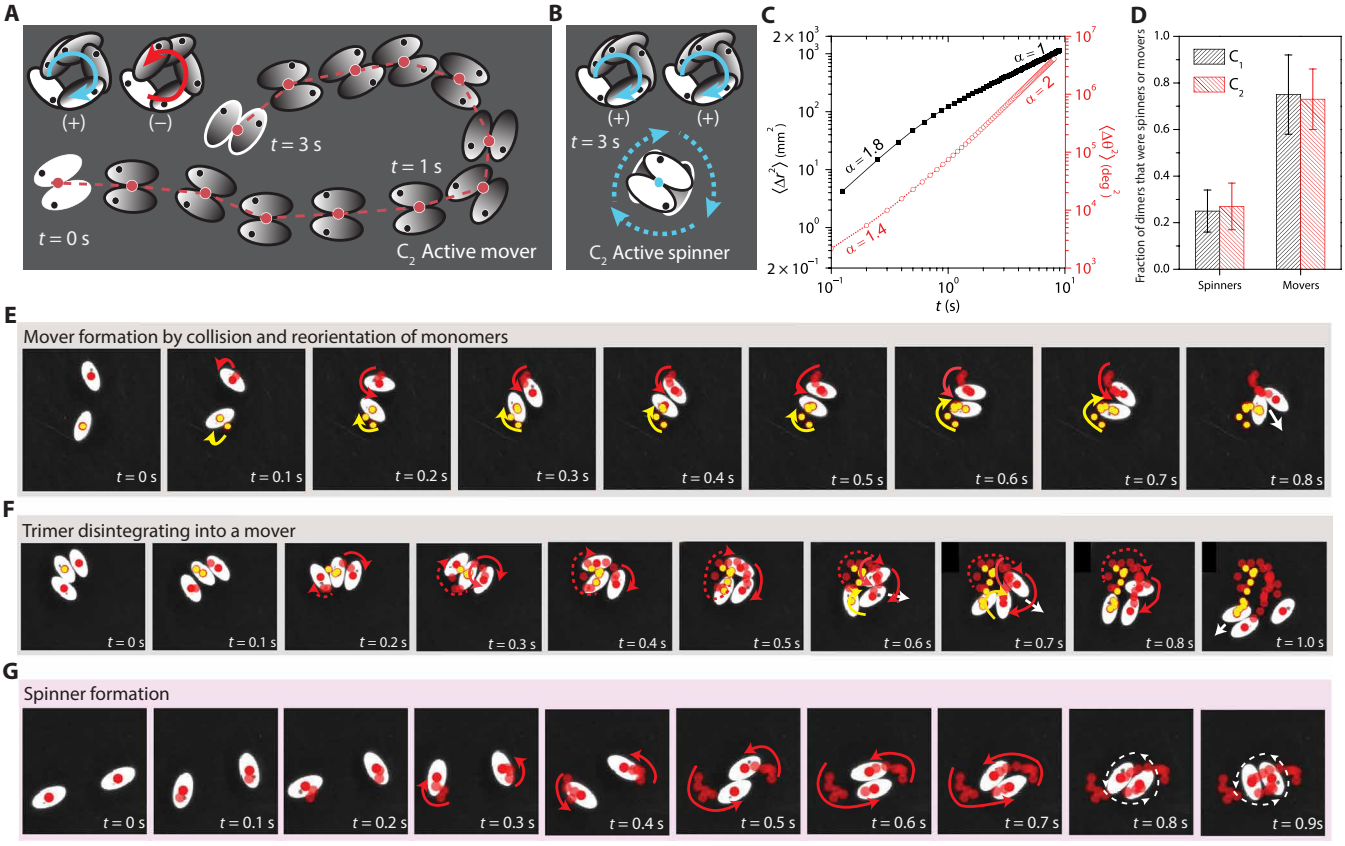

Fig. 2. Emergent stereoselective interactions in polar chiral active ellipsoids. (**A** and **B**) Superimposed snapshots of a representative active mover and spinner, respectively. The mover is composed of a dextrogyre (+) and levogyre (–) monomer [top left in (A)], while the spinner is made of two (+) monomers (B). Note that the spinner has a net clockwise (+) motion (blue dashed arrow), same as that of its components, and is localized in space. (**C**) Translational mean squared displacement (MSD) of mover (black squares) and orientational MSD of spinner (red circles) versus lag time *t*. (**D**) Fraction of dimers that existed as movers and spinners in liquids of C_1 as well as C_2 ellipsoids at $\phi = 1\%$. The error bars represent the SD of the mean and were obtained from multiple statistically independent realizations of an experiment. (**E** to **G**) Pathways of mover and spinner formation. The panels depict the sequence of steps aiding in the dimer formation. A mover bond is typically mediated by two reaction mechanisms. (E) Collision followed by realignment. (F) Trimer disintegration into a mover and monomer. (G) A spinner bond mediated by collision of two aligned particles. All these moves generally last 1 s. Photo credit: (E to G) Pragya Arora, JNCASR.

mixtures of C_1 and C_2 ellipsoids, the mover fraction is nearly three times the spinner fraction—a clear sign of active stereoselectivity (Fig. 2D). For larger *R* (C_3 to C_6 ellipsoids), we exclusively observed only movers, although its lifetime decreased with *R*, since the opposing active torques keeping the monomers together also decreased (movie S4 and fig. S8). The absence of spinners at large *R* is also understandable. For a spinner to be stable, monomers should not slip past each other, and this is possible only when *R* is comparable to the radius of revolution of the monomer about the spinners' COM, which is nothing but $\frac{\beta}{2}$. $R < \frac{\beta}{2}$ for C_1 and C_2 ellipsoids and $R > \frac{\beta}{2}$ for C_3 to C_6 ellipsoids (Table 1).

To understand why movers are more favored over spinners, we investigated the physical mechanisms of dimer formation by closely observing the path traced by the monomers moments before they

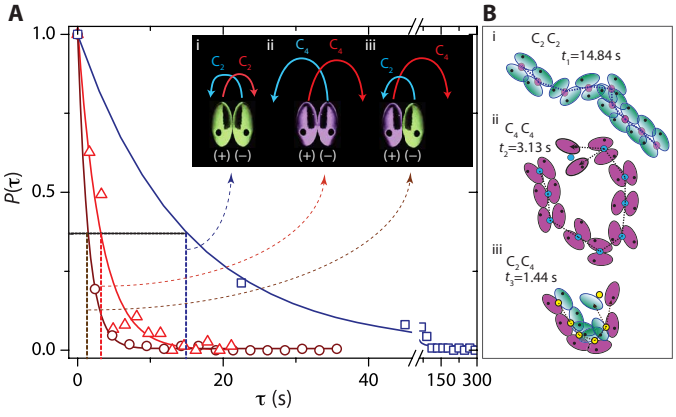

Fig. 3. Self-recognition in polar chiral active ellipsoids. (**A**) Probability distribution of mover lifetimes for the three possible configurations shown in the inset. (i) C_2C_2 (hollow blue squares), (ii) C_4C_4 (red triangles), and (iii) C_2C_4 (brown circles). Both the radius (represented by the arrows in the inset) and the angular velocities of C_2 and C_4 are different. (**B**) Superimposed snapshots of representative active mover trajectory for each of the three configurations. The average lifetime τ_{mov} [shown by dashed vertical lines in (A)] of C_2C_2 mover is 14.8 s, that of C_4C_4 mover is 3.1 s, and that of C_2C_4 mover is 1.4 s. Photo credit: (A) Pragya Arora, JNCASR.

formed the adduct. Snapshots in Fig. 2 (E to G), show the reaction pathways for the mover and spinner formation modes, respectively. Two reaction mechanisms typically mediate a mover bond; the first one is via "collision followed by realignment" in which the formation of the mover bond is aided by multiple collisions and realignments of the constituent monomers (Fig. 2E). The second mode, which also occurred frequently, is via the disintegration of a trimer into a mover and monomer (Fig. 2F). However, a spinner is formed by a single mechanism, i.e., "two-particle collision." As opposed to mover formation, realignments are rare, and the spinner was created only for those collision events where the particles were more or less aligned when coming into contact (Fig. 2G). Clearly, the ease with which movers could form over spinners resulted in the observed stereoselective interactions.

Self-recognition in polar chiral active ellipsoids

We now considered the possibility of this active stereoselective interaction leading to chiral self-recognition (*2*); i.e., in assemblies made of ellipsoids of very different chiral activities, there was a preference in the way particles paired up. We focused on mixtures of C_2 and C_4 ellipsoids, as their dynamics were representative of the limiting cases $R < \frac{\beta}{2}$ and $> \frac{\beta}{2}$, respectively. Movie S5 shows the dynamics of a 1 : 1 mixture of individually racemic C_2 and C_4 ellipsoids at ϕ = 10%. This experiment provided the first cue that there might be some form of self-recognition between particles—we observed C_2C_2 spinners and never any C_4C_4 spinners, as expected, but we also never saw any C_2C_4 spinners. We, however, observed C_2C_2, C_4C_4, and also C_2C_4 movers. Measuring their average lifetimes to determine whether there was self-recognition was difficult at high ϕ owing to their interactions with other particles, and at low ϕ, we could not obtain enough statistics.

To overcome this difficulty, before confining the particles and setting the plate in motion, we manually created one each of the three mover configurations—C_2C_2, C_4C_4, and C_2C_4—by placing the appropriate (+) and (–) monomers side by side (inset to Fig. 3A). This initial configuration helped substantially promote dimerization

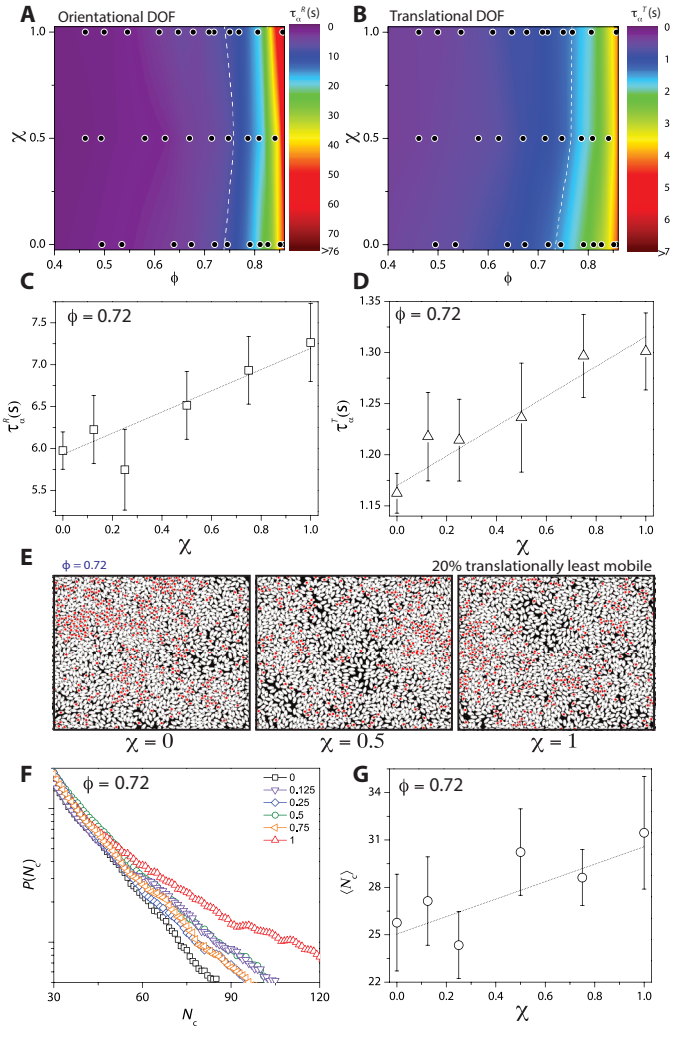

Fig. 4. Relaxation dynamics of polar chiral active liquids depends on their net chirality, χ. (**A** and **B**) Relaxation dynamics phase diagram in the (χ, ϕ) plane for orientational and translational degrees of freedom (DOF), respectively. The circles represent the χ and ϕ at which experiments were performed. In (A) and (B), the isochrones at intermediate ϕ are shown by white dashed lines. The color bar indicates the value of τ_α^R and τ_α^T. τ_α for ϕ's in between experimental data points were obtained from linear interpolation. (**C** and **D**) τ_α^R versus χ and τ_α^T versus χ, respectively, at ϕ = 0.72. (**E**) Top 20% translationally least mobile particles (red filled circles) in a time interval of $5t^*$ across various χ at ϕ = 0.72. (**F**) Probability distribution of cluster size $P(N_c)$ at ϕ = 0.72 across various χ. (**G**) $\langle N_c \rangle$ versus χ for ϕ = 0.72. In (C), (D), and (G), the error bars represent the SD of the mean and were obtained from multiple statistically independent realizations of an experiment. Photo credit: (E) Pragya Arora, JNCASR.

under vertical agitation (movie S6). Trajectories representative of each of the three movers is shown in Fig. 3B. By repeating this experiment a few hundred times, we measured the probability distribution of mover lifetimes, $P(\tau)$, for each of the three movers. $P(\tau)$ was an exponential for all dimer types, and we defined the average lifetime as $P(\tau = \tau_{mov}) = \frac{1}{e}$. These measurements provided the first evidence for chiral self-recognition in active matter: Movers made of like particles were longer-lived in comparison to those made of unlike ones (Fig. 3A). In C_2C_4 movers, besides the radii, the angular velocities of the constituent monomers are also different (Table 1).

The monomers thus slide past each other, and the lifetime of these movers is smaller than even C_4C_4 ones.

Relaxation dynamics depends on the net chirality of active liquids

Having uncovered the active matter analogs of stereoselectivity, we next explored the consequences of these interactions in the dense limit. Unlike in assemblies of C_3 to C_6 ellipsoids, where we never observed spinner states, in liquids of C_1 and C_2 ellipsoids, both movers and spinners exist. Furthermore, in liquids of C_1 and C_2 ellipsoids, even at a fixed ϕ, the net chirality, χ, decides whether movers can even form; in a racemic mixture ($\chi = 0$), both mover and spinner states exist, whereas in an enantiopure liquid ($\chi = 1$), only spinners exist. Here, $\chi = |N_+ - N_-|/N_+ + N_-$, where N_+ and N_- are the fraction of the (+) and (−) monomers, respectively. Since movers and spinners have very distinct dynamics, we naïvely expect that at a fixed ϕ, varying χ alters the nature of relaxation dynamics.

To begin with, we looked for quantifiable differences in the relaxation dynamics of liquids of C_2 ellipsoids across three different net chiralities: $\chi = 1$ [100% (+) monomers], $\chi = 0.5$ [75% (+) monomers and 25% (−) monomers], and $\chi = 0$ [50% (+) monomers and 50% (−) monomers]. We varied ϕ from 0.1 to 0.84 while ensuring that, across χ, the ϕ′s were nearly identical to enable comparison. For all χ, we observed the formation of dynamic aggregates for $\phi \gtrsim 0.2$ (figs. S9 and S10). We, however, did not observe any large-scale phase separation consistent with recent simulation findings on active rods (*27*, *28*). Also, over this range of χ and ϕ values studied, we did not observe segregation of enantiomers (*13*), microflocks with phase-locked dynamics (*18*, *29*), and activity-induced synchronization (*20*). There was no notable difference in the static or dynamical properties of these clusters with χ, and we do not dwell on it here. Next, we quantified the structural relaxation time for the orientational degrees of freedom (DOF), τ_α^R, and the translational DOF, τ_α^T, through their respective time correlators (fig. S11). Like in passive liquids of ellipsoids (*30*), even for our chiral active liquids, at fixed χ and with ϕ, orientational slowing down is more rapid than the translational one—τ_α^R grows by more than two orders of magnitude while τ_α^T grows by one order of magnitude (Fig. 4, A and B, and fig. S12). The isochrones (dashed white lines in Fig. 4, A and B), however, are not parallel to the ordinate but appear curved, suggesting that, at constant ϕ, changing χ alters relaxation dynamics. While interesting, this inference needs to be interpreted with caution due to the limited χ values explored hitherto. This is mainly because the enantiopure ($\chi = 1$) and enantiomeric excess ($\chi = 0.5$) liquids had to be made by manually placing each monomer of the correct handedness, almost 8000 particles for $\phi = 0.84$, on the plate.

To strengthen these findings, for $\phi = 0.72$, we carried out experiments for six values of χ. The effect of changing χ on relaxation dynamics is now clear—both τ_α^R (Fig. 4C) and τ_α^T (Fig. 4D) increase almost linearly with χ, albeit the change in the latter is smaller than in the former. Although the overall growth in τ_α^R and τ_α^T is by ≈20 and ≈10%, respectively, we emphasize that this stems purely from changing χ alone and is indeed unexpected. Since we observed no apparent change in the structure of these liquids, we sought to determine whether the observed slowing down with χ was a consequence of growing dynamical length scales. This line of thinking was motivated by studies on dense supercooled liquids where an increase in the structural relaxation times with density, or on lowering temperature, is accompanied by a growing cooperativity length scale, associated with the size of dynamical heterogeneities, but without any apparent change in static structure (*31*, *32*). Borrowing from these studies, we determined whether dynamics even in our chiral active liquids was spatiotemporally heterogeneous. At $\phi = 0.72$ and for all χ, we quantified the top 20% of the least mobile particles over a time interval $5t^*$, where t^* is the cage rearrangement time (see fig. S13). We found that density relaxation was dynamically heterogeneous and that the least mobile particles were spatially clustered (Fig. 4E). Two least mobile particles were said to belong to the same cluster if one ellipsoid, when expanded 1.4 times the major axis, encompasses the other's center. We then divided the entire experimental data into six statistically independent realizations, and Fig. 4F shows the probability distribution of cluster sizes $P(N_c)$ for one such realization. From $P(N_c)$, we computed the average size of cooperatively rearranging regions $\langle N_c^T \rangle = \frac{\sum N_c^2 P(N_c)}{\sum N_c P(N_c)}$. $\langle N_c \rangle$ grows nearly linearly with χ for $\phi = 0.72$ (Fig. 4F) and is consistent with the observed slowing down of dynamics.

In addition to the least mobile particle clusters, one could equivalently look at the most mobile ones, which are also known to behave in a highly cooperative manner in dense liquids. The evolution of not just the size but also the nature of these dynamical heterogeneities with χ is notable for $\phi \approx 0.85$ (Fig. 5 and movie S7). In the enantiopure liquid (Fig. 5C), these heterogeneities were mostly large spinning vortices composed of almost 200 particles, with the chirality of these vortices being the same as the monomers'. At $\chi = 0$ (Fig. 5A) and $\chi = 0.5$ (Fig. 5B), we observed both (+) and (−) vortices, and these were also smaller in comparison to $\chi = 1$. Besides vortices, we also observed streaming flows like those seen in liquids of achiral active particles (*33*). While orientational relaxation, which requires particles to rotate,

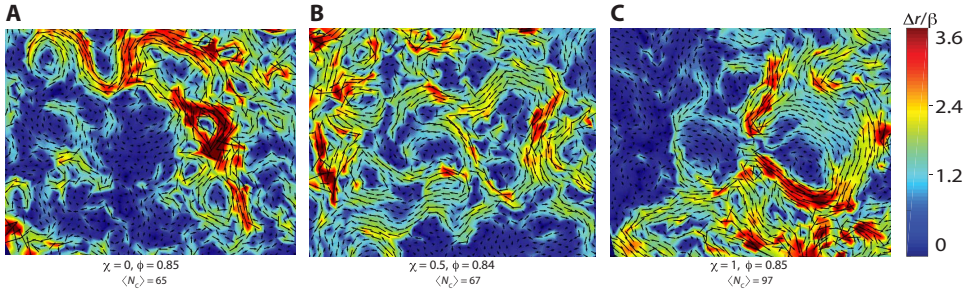

Fig. 5. Chirality-dependent cooperative dynamics. (**A** to **C**) Particle displacement maps over $7t^*$ for $\phi = 0.85$. (A) $\chi = 0$ (racemic mixture). (B) $\chi = 0.5$ (enantiomeric excess). (C) $\chi = 1$ (enantiopure). The color bar shows the magnitude of scaled particle displacement $\Delta r/\beta$ over $7t^*$.

is hindered at these ϕ values, these vortices and streaming flows, which have no counterparts in equilibrium liquids, provide new pathways (*34*) for translational relaxation of structure and is consistent with the observed weak growth in τ_α^T.

DISCUSSION

In summary, our experiments on shape achiral grains with tunable chiral activity has helped uncover the purely dynamical analogs of stereoselectivity and chiral self-recognition. The dynamics of our chiral active liquids is exceptionally rich. Over a window of chiral activities, we observed the formation of homo- and heterochiral dimers with distinct dynamics, and this influenced behavior even in the dense regime. Varying only the total chirality of the active liquids from racemic to enantiomerically pure resulted in dynamical slowing down due to stark changes in the nature of collective relaxation. We anticipate that bringing in complexity in the particle through shape and/or internal DOF will have a profound influence on the emergent behavior of chiral active liquids. It is plausible that, in these systems, active chirality-mediated interactions result in more complex clusters, and their role in emergent dynamics is worthy of investigation. Furthermore, the possibility of tuning particle surface roughness in our approach allows systematically probing the consequences of frictional forces on the clustering mechanisms (*35*). We have shown that, even in systems, where the constituent particles lack attractive interactions (*36*), introducing chiral activity can bring about specificity in interactions, and this can prove to be a powerful route for steering their self-assembly.

MATERIALS AND METHODS

Details of 3D printing

The particles were 3D-printed using the printer model PROJET 3600 MultiJet 3D printer. These particles were designed in MATLAB and AutoCAD software, and the printing procedure required the files in the stereolithographic (.stl) format. The print resolution is 16 μm, which is notably smaller than the size of the particles (~2 to 6 mm) and hence provides control over the surface roughness, allowing us to build parts, patterns, and molds with fine feature details. The printer uses an inkjet printing process that uses piezo printhead technology to deposit a photo-curable plastic resin and a casting wax material layer by layer around the particle. During the print process, one part of the particle is encoded within wax matrix, making it rougher (white part), see fig. S4B, as compared to the other transparent side, thus providing a friction anisotropy by providing differences in surface finish. Although the friction anisotropy in our particles in the present experiments is held the same, our approach allows us to additionally tune the surface roughness by adjusting the extent of the particle encoded within the wax matrix. Around 3000 particles can be fabricated in 3 hours in one batch. They are printed on a tray (shown in fig. S1) and are encased within wax molds, which are stuck to the base of the tray. The post-processing of these particles embedded in a wax mold requires sonication in oil at 60°C; this results in melting of the wax and leaves behind the 3D-printed plastic part. Last, the plastic parts are washed thoroughly with soap and water solution, followed by rinsing with isopropanol and thorough drying. All the particles are identical on visual examination, and the inhomogeneities at the length scale of the particle are expected to be an order of few tens of micrometers.

Measuring vertical and horizontal components of acceleration

A triaxial accelerometer is used to quantify the vibrations at the top of the plate. We measured the vertical and horizontal components of acceleration and found the ratio of these components to be approximately 2% (shown in fig. S2). This value is comparable to those achieved by Harris and Bush (*24*). Thus, the sinusoidal forcing from the shaker is channeled into vertical driving of the plate.

Imaging the particles

The particles are imaged from above with a high-speed camera. A total of 8000 particles were placed on the plate, out of which 1500 particles lying within the central region were imaged (see the red box in fig. S3). By imaging the central region approximately 20 to 30 $\sigma\left(\sigma = \frac{\alpha+\beta}{2}\right)$ away from the edges of the flower boundary, we excluded the boundary effects.

SUPPLEMENTARY MATERIALS

Supplementary material for this article is available at http://advances.sciencemag.org/cgi/content/full/7/9/eabd0331/DC1

REFERENCES AND NOTES

1. S. M. Morrow, A. J. Bissette, S. P. Fletcher, Transmission of chirality through space and across length scales. *Nat. Nanotechnol.* **12**, 410–419 (2017).
2. H. Jędrzejewska, A. Szumna, Making a right or left choice: Chiral self-sorting as a tool for the formation of discrete complex structures. *Chem. Rev.* **117**, 4863–4899 (2017).
3. G. Kokot, S. Das, R. G. Winkler, G. Gompper, I. S. Aranson, A. Snezhko, Active turbulence in a gas of self-assembled spinners. *Proc. Natl. Acad. Sci. U.S.A.* **114**, 12870–12875 (2017).
4. V. Soni, E. S. Bililign, S. Magkiriadou, S. Sacanna, D. Bartolo, M. J. Shelley, W. T. M. Irvine, The odd free surface flows of a colloidal chiral fluid. *Nat. Phys.* **15**, 1188–1194 (2019).
5. B. A. Grzybowski, G. M. Whitesides, Dynamic aggregation of chiral spinners. *Science* **296**, 718–721 (2002).
6. A. P. Petroff, X.-L. Wu, A. Libchaber, Fast-moving bacteria self-organize into active two-dimensional crystals of rotating cells. *Phys. Rev. Lett.* **114**, 158102 (2015).
7. E. Lauga, W. R. DiLuzio, G. M. Whitesides, H. A. Stone, Swimming in circles: Motion of bacteria near solid boundaries. *Biophys. J.* **90**, 400–412 (2006).
8. H. S. Jennings, On the significance of the spiral swimming of organisms. *Am. Nat.* **35**, 369–378 (1901).
9. T.-W. Su, L. Xue, A. Ozcan, High-throughput lensfree 3D tracking of human sperms reveals rare statistics of helical trajectories. *Proc. Natl. Acad. Sci. U.S.A.* **109**, 16018–16022 (2012).
10. J.-C. Tsai, F. Ye, J. Rodriguez, J. P. Gollub, T. C. Lubensky, A chiral granular gas. *Phys. Rev. Lett.* **94**, 214301 (2005).
11. F. Kümmel, B. ten Hagen, R. Wittkowski, I. Buttinoni, R. Eichhorn, G. Volpe, H. Löwen, C. Bechinger, Circular motion of asymmetric self-propelling particles. *Phys. Rev. Lett.* **110**, 198302 (2013).
12. M. Workamp, G. Ramirez, K. E. Daniels, J. A. Dijksman, Symmetry-reversals in chiral active matter. *Soft Matter* **14**, 5572–5580 (2018).
13. C. Scholz, M. Engel, T. Pöschel, Rotating robots move collectively and self-organize. *Nat. Commun.* **9**, 931 (2018).
14. M. C. Marchetti, J. F. Joanny, S. Ramaswamy, T. B. Liverpool, J. Prost, M. Rao, R. A. Simha, Hydrodynamics of soft active matter. *Rev. Mod. Phys.* **85**, 1143–1189 (2013).
15. H. Löwen, Chirality in microswimmer motion: From circle swimmers to active turbulence. *Eur. Phys. J. Spec. Top.* **225**, 2319–2331 (2016).
16. J. Palacci, S. Sacanna, A. P. Steinberg, D. J. Pine, P. M. Chaikin, Living crystals of light-activated colloidal surfers. *Science* **339**, 936–940 (2013).
17. M. E. Cates, J. Tailleur, Motility-induced phase separation. *Annu. Rev. Condens. Matter Phys.* **6**, 219–244 (2015).
18. B. Liebchen, D. Levis, Collective behavior of chiral active matter: Pattern formation and enhanced flocking. *Phys. Rev. Lett.* **119**, 058002 (2017).
19. Q.-L. Lei, M. P. Ciamarra, R. Ni, Nonequilibrium strongly hyperuniform fluids of circle active particles with large local density fluctuations. *Sci. Adv.* **5**, eaau7423 (2019).
20. D. Levis, I. Pagonabarraga, B. Liebchen, Activity induced synchronization: Mutual flocking and chiral self-sorting. *Phys. Rev. Lett.* **1**, 023026 (2019).
21. A. Kudrolli, G. Lumay, D. Volfson, L. S. Tsimring, Swarming and swirling in self-propelled polar granular rods. *Phys. Rev. Lett.* **100**, 058001 (2008).
22. J. Deseigne, O. Dauchot, H. Chaté, Collective motion of vibrated polar disks. *Phys. Rev. Lett.* **105**, 098001 (2010).

23. N. Kumar, H. Soni, S. Ramaswamy, A. K. Sood, Flocking at a distance in active granular matter. *Nat. Commun.* **5**, 4688 (2014).
24. D. M. Harris, J. W. M. Bush, Generating uniaxial vibration with an electrodynamic shaker and external air bearing. *J. Sound Vib.* **334**, 255–269 (2015).
25. C. Bechinger, R. di Leonardo, H. Löwen, C. Reichhardt, G. Volpe, G. Volpe, Active particles in complex and crowded environments. *Rev. Mod. Phys.* **88**, 045006 (2016).
26. Y. Fily, A. Baskaran, M. C. Marchetti, Cooperative self-propulsion of active and passive rotors. *Soft Matter* **8**, 3002–3009 (2012).
27. R. van Damme, J. Rodenburg, R. van Roij, M. Dijkstra, Interparticle torques suppress motility-induced phase separation for rodlike particles. *J. Chem. Phys.* **150**, 164501 (2019).
28. M. Bär, R. Großmann, S. Heidenreich, F. Peruani, Self-propelled rods: Insights and perspectives for active matter. *Ann. Rev. Condens. Matter Phys.* **11**, 441–466 (2020).
29. D. Levis, B. Liebchen, Micro-flock patterns and macro-clusters in chiral active Brownian disks. *J. Phys. Condens. Matter* **30**, 084001 (2018).
30. Z. Zheng, F. Wang, Y. Han, Glass transitions in quasi-two-dimensional suspensions of colloidal ellipsoids. *Phys. Rev. Lett.* **107**, 065702 (2011).
31. E. R. Weeks, J. C. Crocker, A. C. Levitt, A. Schofield, D. A. Weitz, Three-dimensional direct imaging of structural relaxation near the colloidal glass transition. *Science* **287**, 627–631 (2000).
32. S. Gokhale, A. K. Sood, R. Ganapathy, Deconstructing the glass transition through critical experiments on colloids. *Adv. Phys.* **65**, 363–452 (2016).
33. S. P. Thampi, R. Golestanian, J. M. Yeomans, Vorticity, defects and correlations in active turbulence. *Philos. Trans. A Math. Phys. Eng. Sci.* **372**, 20130366 (2014).
34. L. Berthier, Nonequilibrium glassy dynamics of self-propelled hard disks. *Phys. Rev. Lett.* **112**, 220602 (2014).
35. P. Nie, J. Chattoraj, A. Piscitelli, P. Doyle, R. Ni, M. P. Ciamarra, Frictional active Brownian particles. *Phys. Rev. Lett.* **102**, 032612 (2020).
36. M. X. Lim, A. Souslov, V. Vitelli, H. M. Jaeger, Cluster formation by acoustic forces and active fluctuations in levitated granular matter. *Nat. Phys.* **15**, 460–464 (2019).

Acknowledgments: We thank S. Gokhale for critical feedback on our manuscript. **Funding:** A.K.S. thanks the Department of Science and Technology (DST), Government of India, for a Year of Science Fellowship. R.G. thanks DST-SwarnaJayanti fellowship (2016–2021) for financial support. **Author contributions:** P.A. and R.G. conceived the research and designed the experiments. P.A. performed the experiments and carried out data analysis. A.K.S. contributed to project development and provided inputs with the manuscript. R.G. steered the research and wrote the paper with P.A. **Competing interests:** The authors declare that they have no competing interests. **Data and materials availability:** All data needed to evaluate the conclusions in the paper are present in the paper and/or the Supplementary Materials. Additional data related to this paper may be requested from the authors.

Submitted 27 May 2020
Accepted 13 January 2021
Published 26 February 2021
10.1126/sciadv.abd0331

Citation: P. Arora, A. K. Sood, R. Ganapathy, Emergent stereoselective interactions and self-recognition in polar chiral active ellipsoids. *Sci. Adv.* **7**, eabd0331 (2021).

Emergent stereoselective interactions and self-recognition in polar chiral active ellipsoids

Pragya Arora, A. K. Sood and Rajesh Ganapathy

Sci Adv **7** (9), eabd0331.
DOI: 10.1126/sciadv.abd0331